Earth's Future

Key Points:
- Models project higher risk of soil moisture droughts like the recent event in southwestern North America by 2100
- Climate mitigation minimally reduces 21-year drought risk because half the ensemble projects large precipitation declines in all scenarios
- Mitigation reduces the magnitude of extreme single-year droughts, even during longer events, making high-risk droughts less severe

Correspondence to:
B. I. Cook,
benjamin.i.cook@nasa.gov

Uncertainties, Limits, and Benefits of Climate Change Mitigation for Soil Moisture Drought in Southwestern North America

B. I. Cook[1,2] [iD], **J. S. Mankin[2,3]** [iD], **A. P. Williams[2,4]** [iD], **K. D. Marvel[1,5]** [iD], **J. E. Smerdon[2]** [iD], and **H. Liu[2]** [iD]

[1]NASA Goddard Institute for Space Studies, New York, NY, USA, [2]Lamont-Doherty Earth Observatory, Columbia University, Palisades, NY, USA, [3]Department of Geography, Dartmouth College, Hanover, NH, USA, [4]Department of Geography, University of California, Los Angeles, Los Angeles, CA, USA, [5]Center for Climate Systems Research, Columbia University, New York, NY, USA

Abstract Over the last two decades, southwestern North America (SWNA) has been in the grip of one of the most severe droughts of the last 1,200 years, with one third to nearly one half of its severity attributable to climate change. We analyze how the risk of extreme soil moisture droughts in SWNA, analogous to the most severe 21-year ($\geq$ in magnitude to 2000–2020) and single-year ($\geq$ in magnitude to 2002) events of the last several decades, changes in projections from Phase 6 of the Coupled Model Intercomparison Project. By the end of the 21st century, SWNA experiences robust ($R \geq 0.80$) soil moisture drying and substantial increases in extreme single-year drought risk that scale strongly with warming, spanning an 8%–26% probability of occurrence across +2–4 K. Notably, our results show that 21-year droughts analogous to 2000–2020 are up to 5 times more likely than extreme single-year droughts under all levels of warming ($\approx$50%). These high levels of 21-year drought risk are largely invariant across scenarios because of large spring precipitation declines in half the models, shifting SWNA into a drier mean state. Despite projections of this sweeping and ostensibly inevitable increase in 21-year drought risk, climate mitigation reduces their severity by reducing the magnitude of extreme single-year droughts during these events. Our results emphasize both the importance of preparing SWNA for imminent increases in persistent drought events and constraining projected precipitation uncertainty to better resolve future long-term drought risk.

Plain Language Summary Drought is an important natural hazard in southwestern North America, and there is strong evidence that climate change is already increasing the severity of droughts in the region. Using the latest, state-of-the-art climate change projections, we find that warming in the future will increase the risk of both extreme single-year and 21-year soil moisture droughts that are similar to major events of the last two decades. Furthermore, we show that while the magnitude of warming has a strong influence on single-year droughts, even modest warming is likely to lock in an approximately 50% chance of a 21-year drought similar to 2000–2020 by the end of the 21st century. The high levels of 21-year drought risk are driven by large precipitation declines in half the models, which shift the region to a drier mean state under even the lowest warming scenario. Despite the apparent insensitivity of 21-year drought risk to mitigation measures, our results still demonstrate the value of climate change mitigation for reducing future drought severity and single-year extreme drought risk in the region. Our study also highlights the importance of precipitation responses in the models as major uncertainties that must be resolved to increase our confidence in these projections.

1. Introduction

As of spring 2021, much of western North America remains in the grip of a severe, multi-decadal drought event (National Drought Mitigation Center, 2021) that started at the beginning of the 21st century (Delworth et al., 2015; Seager, 2007; Williams et al., 2020). Centered in southwestern North America (SWNA: 125°W–105°W, 30°N–45°N), this drought has caused severe declines in above- and below-ground water resources (Faunt et al., 2016; Overpeck & Udall, 2020; Thomas et al., 2017; Udall & Overpeck, 2017; Xiao et al., 2017, 2018); major agricultural and economic losses (Cooley et al., 2015; Diersen, 2003; Tronstad &
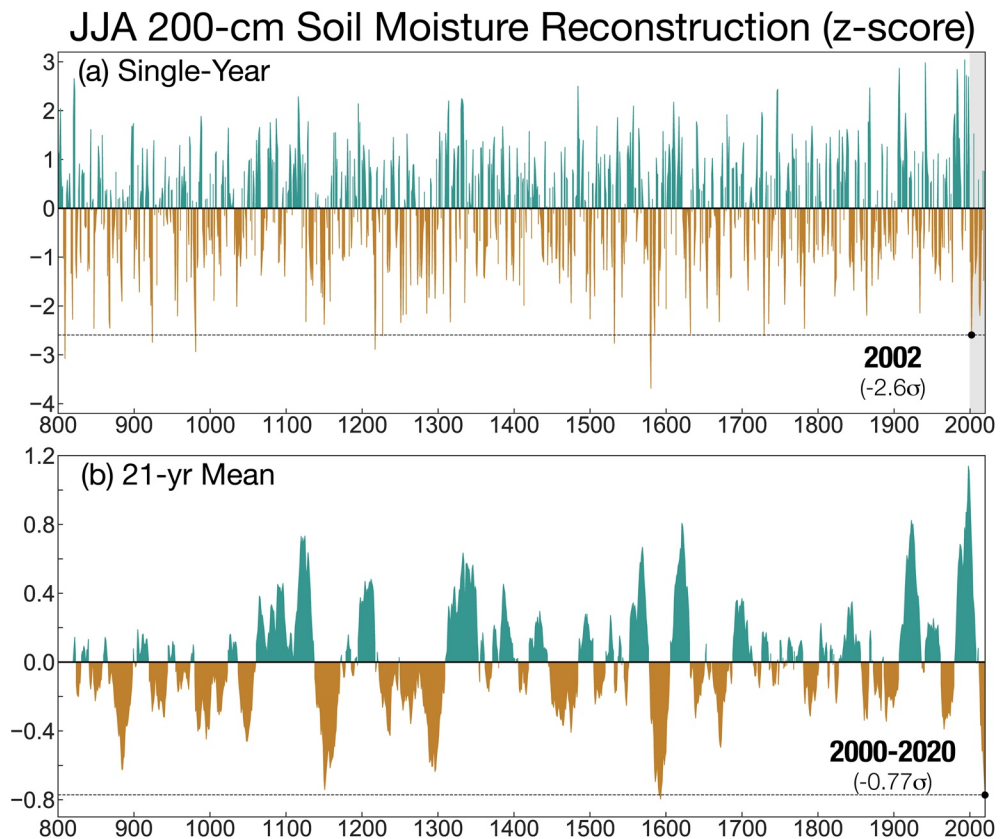
Figure 1. Regional average single-year (a) and 21-year trailing mean (b) soil moisture index values (z-score) from the updated version of the Williams et al. (2020) 0–200 cm soil moisture reconstruction for southwestern North America (125°W–105°W, 30°N–45°N). The extreme droughts used for the analog analyses in this study (2002 for single-year, 2000–2020 for 21-year) are marked by the black dots and dotted lines in each panel. The gray shading in (a) highlights the single-year values included in the 2000–2020 average.

Feuz, 2002); widespread ecosystem disruptions (Anderegg et al., 2013; Fettig et al., 2019; Ganey & Vojta, 2011; Schwalm et al., 2012; Williams et al., 2013); and rapid increases in annual forest fire area (Abatzoglou & Williams, 2016). While such persistent multi-decadal droughts, often termed megadroughts, are common in the paleoclimate record (Cook et al., 2016), this ongoing event is unprecedented in the instrumental period and is the second most severe 21-year drought period of the last 1,200 years (Figure 1; updated soil moisture reconstruction from Williams et al. (2020)).

The 2000–2020 drought was likely triggered by precipitation deficits connected to natural variability and ocean dynamics in the tropical Pacific (Delworth et al., 2015; Lehner et al., 2018; Seager, 2007). However, recent work has attributed one third to nearly one half the severity of the associated soil moisture deficits to climate change through anthropogenically driven increases in evaporative demand (Williams et al., 2020). Such a large contribution from warming is consistent with conclusions from other studies demonstrating that climate change has intensified soil moisture, streamflow, and snow droughts in the western US (Berg & Hall, 2017; Marlier et al., 2017; McCabe et al., 2017; Mote et al., 2016, 2018; Williams et al., 2015; Woodhouse et al., 2016; Xiao et al., 2018). It is also consistent with climate change projections indicating that future warming will continue to exacerbate drought in the region (Ault, 2020; Cook et al., 2015, 2018, 2019, 2020; Overpeck & Udall, 2020; Spinoni et al., 2020; Zhao et al., 2020). Beyond these fundamental expectations of a warmer and drier future, however, there remain some significant uncertainties regarding how climate change will affect drought dynamics. These include how future drying will compare to droughts in the instrumental and paleoclimate record; how various processes, including precipitation and evaporative demand, will ultimately contribute to droughts in the region; how responses of short- (≤1 year) and long- (≥

10 years) term drought events may differ; and the effectiveness of climate change mitigation for ameliorating future drought risk and severity.

We use the latest state-of-the-art climate model simulations from Phase 6 of the Coupled Model Intercomparison Project (CMIP6) (Eyring et al., 2016) and an update of the Williams et al. (2020) soil moisture reconstruction to investigate how the risk and severity of both short- and long-term soil moisture droughts in SWNA will change with warming at the end of the 21st century. This updated reconstruction targets the same soil moisture data set as in Williams et al. (2020), with the following exceptions. First, observational values are now available through summer 2020. Second, humidity data in the US were replaced with the latest version from the Parameter-elevation Regressions on Independent Slopes Model (PRISM) climate datasets (https://prism.oregonstate.edu/notices/notice_20191029.php). Third, precipitation and temperature data for locations outside the US were replaced with the latest version of the Climate Research Unit climate grids (https://crudata.uea.ac.uk/cru/data/hrg/cru_ts_4.04/).

We focus on analogs of two recent events to analyze in these simulations: the 21-year drought that began in 2000 and is ongoing as of spring 2021, and the single most extreme drought year during this period, 2002. We evaluate how droughts equal or greater in magnitude to these recent events are likely to change under a range of warming scenarios, focusing on three primary research questions: (a) How does soil moisture drought change with warming in the CMIP6 projections and how do the projections compare to drought variability over the last 1,200 years?; (b) How do the risks for events that are equal or greater in magnitude to 2002 and 2000–2020 change with warming, and what are the driving processes?; and (c) To what extent can climate mitigation reduce the risk of the single- and 21-year drought analogs that we investigate?

2. Materials and Methods

2.1. Soil Moisture Reconstruction

We assessed drought variability in the instrumental and paleoclimate record using an updated version of the summer season (June-July-August; JJA) 0–200 cm soil moisture reconstruction from Williams et al. (2020). This tree-ring based reconstruction spans 800–2020 C.E. and targets 0–200 cm soil moisture estimates from an empirically constrained model that accounts for inputs from precipitation, losses via evapotranspiration, and carryover storage between seasons. The reconstruction has high skill over SWNA, with average cross validation $R^2 > 0.80$ after 1400 C.E. and $R^2 > 0.70$ back to 800 C.E. We use the SWNA regional average (125°–105°W, 30°–45°N) time series from the reconstruction for comparison with the CMIP6 simulations, using the tree-ring reconstructed values for 800–1900 C.E. and direct instrumental values for 1901–2020. Soil moisture units are in standardized z-scores with unit standard deviation (σ), and the regionally averaged reconstruction is calibrated to the observed mean and variance during 1901–1983.

We analyzed drought analogs based on the most recent drought period in this reconstruction through summer of 2020, an extended version of the event that was the focus of the Williams et al. (2020) study (Figure 1). For extreme single-year droughts, we used 2002 as our analog, the single driest year of the last several decades with a soil moisture anomaly of -2.6σ, ranking as the 9th driest year in the full reconstruction back to 800 C.E. We also analyzed changes in 21-year drought events using the the 21-year mean soil moisture from 2000–2020, which had a magnitude of -0.77σ and was tied with the late 16th-century megadrought as the second driest 21-year soil moisture anomaly since 800 C.E. While the degree to which such rankings are statistically distinguishable is sensitive to various uncertainties, the reconstruction nevertheless highlights the exceptional nature of recent drought in SWNA.

2.2. CMIP6 Multi-Model Ensemble

We used climate model simulations from the CMIP6 database, a set of standardized experiments contributed by climate modeling groups from around the world (Eyring et al., 2016). We analyzed the "historical" (1850–2014) simulations conducted as part of the core "DECK" experiments (Eyring et al., 2016) and three forcing scenarios ("Shared Socioeconomic Pathways"; SSPs) for the 21st century (2015–2100) from ScenarioMIP (O'Neill et al., 2016). The historical simulations used estimates of natural (e.g., volcanic eruptions, solar, and orbital variability) and anthropogenic (e.g., greenhouse gas emissions, aerosols, land use change)

Table 1

Models Used to Construct the CMIP6 Multi-Model Ensemble, Including the Ensemble Member Used, the Estimated Equilibrium Climate Sensitivity (ECS), and the Reference for Submission of These Simulations to CMIP6

| Model	Ensemble	ECS (K/2 × CO_2)	Reference
ACCESS-CM2	r1i1p1f1	4.7	Dix et al. (2019a); Dix et al. (2019b)
ACCESS-ESM1-5	r1i1p1f1	3.9	Ziehn et al. (2019a); Ziehn et al. (2019b)
BCC-CSM2-MR	r1i1p1f1	3.0	Wu et al. (2018), Xin et al. (2019)
CanESM5	r1i1p1f1	5.6	Swart et al. (2019a); Swart et al. (2019b)
CESM2	r1i1p1f1	5.2	Danabasoglu (2019a)
CESM2-WACCM	r1i1p1f1	4.8	Danabasoglu (2019b); Danabasoglu (2019c)
CNRM-CM6-1	r1i1p1f2	4.8	Voldoire (2018); Voldoire (2019)
CNRM-ESM2-1	r1i1p1f2	4.8	Seferian (2018); Seferian (2019)
EC-Earth3-Veg	r1i1p1f1	4.3	EC-Earth Consortium (EC-Earth) (2019a); EC-Earth Consortium (EC-Earth) (2019b)
GISS-E2-1-G	r1i1p3f1	2.7	NASA Goddard Institute for Space Studies (NASA/GISS) (2018); NASA Goddard Institute for Space Studies (NASA/GISS) (2020)
IPSL-CM6A-LR	r1i1p1f1	4.6	Boucher et al. (2018); Boucher et al. (2019)
KACE-1-0-G	r2i1p1f1	4.5	Byun, Lim, Sung, et al. (2019); Byun, Lim, Shim, et al. (2019)
MIROC6	r1i1p1f1	2.6	Shiogama et al. (2019), Tatebe and Watanabe (2018)
MPI-ESM1-2-LR	r1i1p1f1	3.0	Wieners et al. (2019a); Wieners et al. (2019b)
MPI-ESM1-2-HR	r1i1p1f1	3.0	Jungclaus et al. (2019), Schupfner et al. (2019)
MRI-ESM2-0	r1i1p1f1	3.2	Yukimoto et al. (2019a); Yukimoto et al. (2019b)
NorESM2-MM	r1i1p1f1	2.5	Bentsen et al. (2019a); Bentsen et al. (2019b)
UKESM1-0-LL	r1i1p1f2	5.3	Tang et al. (2019); Good et al. (2019)

Note. All ECS values were sourced from Meehl et al. (2020).

climate forcings to simulate climate change and variability over the instrumental period, while the SSP projections are based on scenarios of greenhouse gases and other forcings consistent with various assumptions regarding possible trajectories of economic growth, energy use, climate mitigation efforts, and global governance. The three SSPs we employed are taken from Tier 1 of ScenarioMIP and span a range of forcing and warming levels: SSP1-2.6 (+2.6 W m^{-2} radiative imbalance at the end of the 21st century; low forcing sustainability pathway), SSP2-4.5 (+4.5 W m^{-2}; medium forcing middle-of-the-road pathway), and SSP3-7.0 (+7.0 W m^{-2}; medium- to high-end forcing pathway).

We constructed our 18-member multi-model ensemble (MME; summarized in Table 1) by selecting models that provided the mrsol variable (in each soil layer, the mass of water in all phases, including ice; kg m^{-2}) for continuous ensemble members from the historical simulations through all three SSP scenarios (1850–2100). We used a single realization from each model, and all models are equally represented within and across the three SSP scenarios. Where available, we also analyzed the following diagnostics within the MME: tas (2-m near surface air temperature; K), pr (precipitation rate, all phases; mm day^{-1}), hurs (near-surface relative humidy; percent), and mrro (total runoff, including drainage through the base of the soil model; mm day^{-1}). Global warming levels in our ensembles relative to the 1851–1880 near pre-industrial baseline are presented in Figure 2. The three SSPs cover a range of warming levels in the latter part of the 21st century (2071–2100), with MME median warming of +2.1 K (SSP1-2.6), +2.9 K (SSP2-4.5), and +3.9 K (SSP3-7.0).

2.3. CMIP6 Postprocessing and Analyses

To facilitate comparisons with the 0–200 cm JJA tree-ring based soil moisture reconstruction, we post-processed the individual-layer soil moisture in mrsol by interpolating to 200 cm and standardizing the resulting time series to match the mean and variability in the reconstruction. For every month, we integrated each model's soil moisture from the surface through all layers where the bottom layer depth was above 200 cm.

Global Surface Air Temperature Anomalies
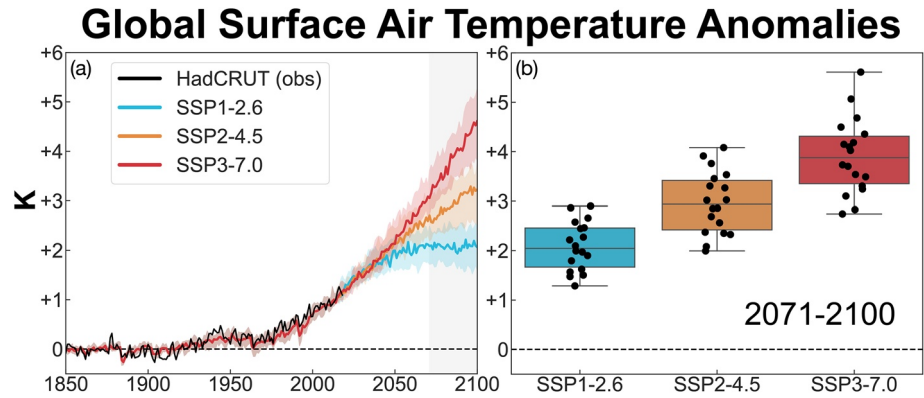
Figure 2. Global annual average surface air temperature anomalies (K) in the CMIP6 18-member multi-model ensemble (MME) used in our study. Anomalies are calculated using an approximate pre-industrial baseline (1851–1880). (a) Time evolution of temperature anomalies in observations (black line, 1851–2018; HadCRUT5 (Morice et al., 2020)) and each shared socioeconomic pathway (SSP) in the MME (ensemble median in solid lines; colored shading delineates the MME interquartile range within each SSP). Gray shading is the 2071–2100 interval. (b) Warming across the MME for each SSP in 2071–2100. Whiskers encompass the full range across the ensemble, and values for individual models are in the black dots.

We then added a fractional estimate of soil moisture from the next layer that includes 200 cm based on its relative depth in that layer. Second, we calculated summer season average soil moisture by averaging the 200-cm interpolated soil moisture across JJA, and then calculated a land-area weighted average of the JJA mean over the same spatial domain as the SWNA reconstruction time series (125°W–105°W, 30°N–45°N). Finally, we rescaled the 200 cm JJA soil moisture from each model to match the mean and variability of the SWNA reconstruction over 1851–1950. We also used tas and hurs from CMIP6 to calculate the vapor pressure deficit (VPD) for each grid cell and month individually. We approximated the saturation vapor pressure using:

$$e_s = e_0 * exp\left[\frac{L}{R_v} * \left(\frac{1}{T_0} - \frac{1}{T}\right)\right] \tag{1}$$

where e_s is saturation vapor pressure (kPa), $e_0 = 0.6113$ kPa, $R_v = 461\ J \times K^{-1} \times kg^{-1}$, $T_0 = 273.15\ K$, and T is the temperature (K; using tas). We then calculated actual vapor pressure (e_a) as the product of hurs and e_s (after converting % hurs values to fractional values), and the vapor pressure deficit as e_s minus e_a.

2.4. Analyses

The bulk of our analyses are focused on regional average soil moisture time series for SWNA from the CMIP6 models. We acknowledge that this broad region encompasses a diversity of environments and ecosystems, and that such large-scale averaging may mask over important sub-regional heterogeneity in drought responses to climate change. This averaging is necessary, however, to provide consistent time series for comparison with the reconstruction of Williams et al. (2020), which is used to (a) define the drought analogs we are investigating and (b) establish the baseline of historical drought variability against which the CMIP6 projections are evaluated. We nevertheless also show spatial maps of the MME mean response in the CMIP6 models to communicate spatially heterogenous drought responses within SWNA and to put the changes in the region in the context of changes across North America.

To analyze spatially explicit changes in the MME mean, we equally weighted each model and averaged all models and years for two thirty-year periods: 2071–2100 and 1971–2000. We then calculated the difference at each grid cell (2071–2100 minus 1971–2000) and assessed robustness in the ensemble response using the robustness metric R from Knutti and Sedlacek (2013), which incorporates information on the magnitude and sign of the MME change, variability within each simulation, and the spread across models. A higher model spread or smaller signal will decrease R. Values of R will increase if the mean, shape of the

distribution, or variability changes between the two time periods. A value of $R = 1.0$ indicates perfect agreement across models in the ensemble response. For this study, we used a robustness threshold of $R \geq 0.80$, which Knutti and Sedlacek (2013) referred to as "good agreement." Values below this threshold, indicating non-robust responses, are shaded by diagonal hatching.

To investigate changes in drought risk, we analyzed the annually resolved SWNA time series and a smoothed version with a 21-year running mean applied in the reconstruction and models. We used the annual time series to investigate changes in the risk of single-year drought events equal to or drier than 2002 in the observed record (-2.6σ) in the CMIP6 projections. Similarly, we used the 21-year smoothed time series to investigate how 21-year drought events with trailing mean values equal to or drier than 2000–2020 (-0.77σ) change with warming. The trailing mean in the models is calculated so that 2071 (the first year of the late 21st century period we analyze) is the mean of 2051–2071, the value for 2072 is the mean of 2052–2072, and so forth to the final year 2100, which is the mean of 2080–2100. We calculated "risk" as the fraction of years within the reconstruction or MME with values matching or exceeding the magnitude of the 2002 and 2000–2020 droughts from the reconstruction. In the MME, we do this calculation for the historical (1851–2020) and late 21st century (2071–2100) time periods, pooling together all years and models together during these intervals.

3. Results

3.1. Drought Mechanisms in Climate Model Projections

Projected changes in soil moisture and runoff drought in response to increased greenhouse gas warming depend largely on changes in evapotranspiration and precipitation. Increased evapotranspiration is a major driver of projected drying trends in many regions, occurring in response to strong warming (Knutti & Sedlacek, 2013) and increased evaporative demand (Ault et al., 2016; Cook et al., 2014, 2015; Scheff & Frierson, 2013) in all seasons and regions. Uncertainties in actual evapotranspiration changes, and their contribution to surface drying, are largely attributable to how plant water use changes in response to warming and increased carbon dioxide concentrations, with plants acting to either ameliorate (Swann et al., 2016, 2018) or amplify (Mankin et al., 2018, 2019) surface water losses. There are also large uncertainties in precipitation within climate model projections, with often large seasonal and spatial differences in the sign, magnitude, and robustness of responses (Knutti & Sedlacek, 2013) and a strong influence of internal climate variability (Mankin et al., 2020). Total precipitation responses to warming may therefore increase or decrease drought severity and risk, depending on the region and season analyzed, though in many cases even large increases in precipitation are unlikely to completely negate warming-driven increases in evapotranspiration (Cook et al., 2020). Beyond changes in total precipitation, warming also increases the fraction of precipitation falling as rain rather than snow (Krasting et al., 2013; Mankin & Diffenbaugh, 2015), causes earlier melting of the snowpack (Musselman et al., 2021), and reduces total snowpack water storage (Mote et al., 2018; Shi & Wang, 2015). Such shifts can lead to significant seasonal changes in both runoff (Li et al., 2017; Mankin et al., 2015) and soil moisture (Gergel et al., 2017; Harpold et al., 2015; Marvel et al., in review), even if changes in total precipitation are negligible. More detailed analyses of seasonal changes in important hydrologic variables in the CMIP6 projections across our study region are provided in Marvel et al (in review).

### 3.2. Precipitation and Vapor Pressure Deficit

As in the previous generations of climate models (Knutti & Sedlacek, 2013), the sign, magnitude, and robustness of precipitation responses to warming in our MME is highly variable across regions and seasons (Figure 3), and largely consistent with other CMIP6 analyses (Cook et al., 2020; Ukkola et al., 2020). The strongest, most robust increases in precipitation occur in northern and eastern North America during winter (December-January-February; DJF) and spring (March-April-May; MAM) and across Mexico in the fall (September-October-November; SON). Robust precipitation declines are not nearly as extensive, limited to the southwestern US in spring; in Mexico in winter, spring, and fall; and in a band across the Pacific Northwest, Northern Plains, and Midwest in the summer. Over SWNA (dashed black box), robust precipitation increases are confined primarily to the northern half of the domain during the winter, along with more modest increases during summer under the strongest warming scenario. Robust declines in precipitation

∆Precipitation, 2071-2100 (mm/day)
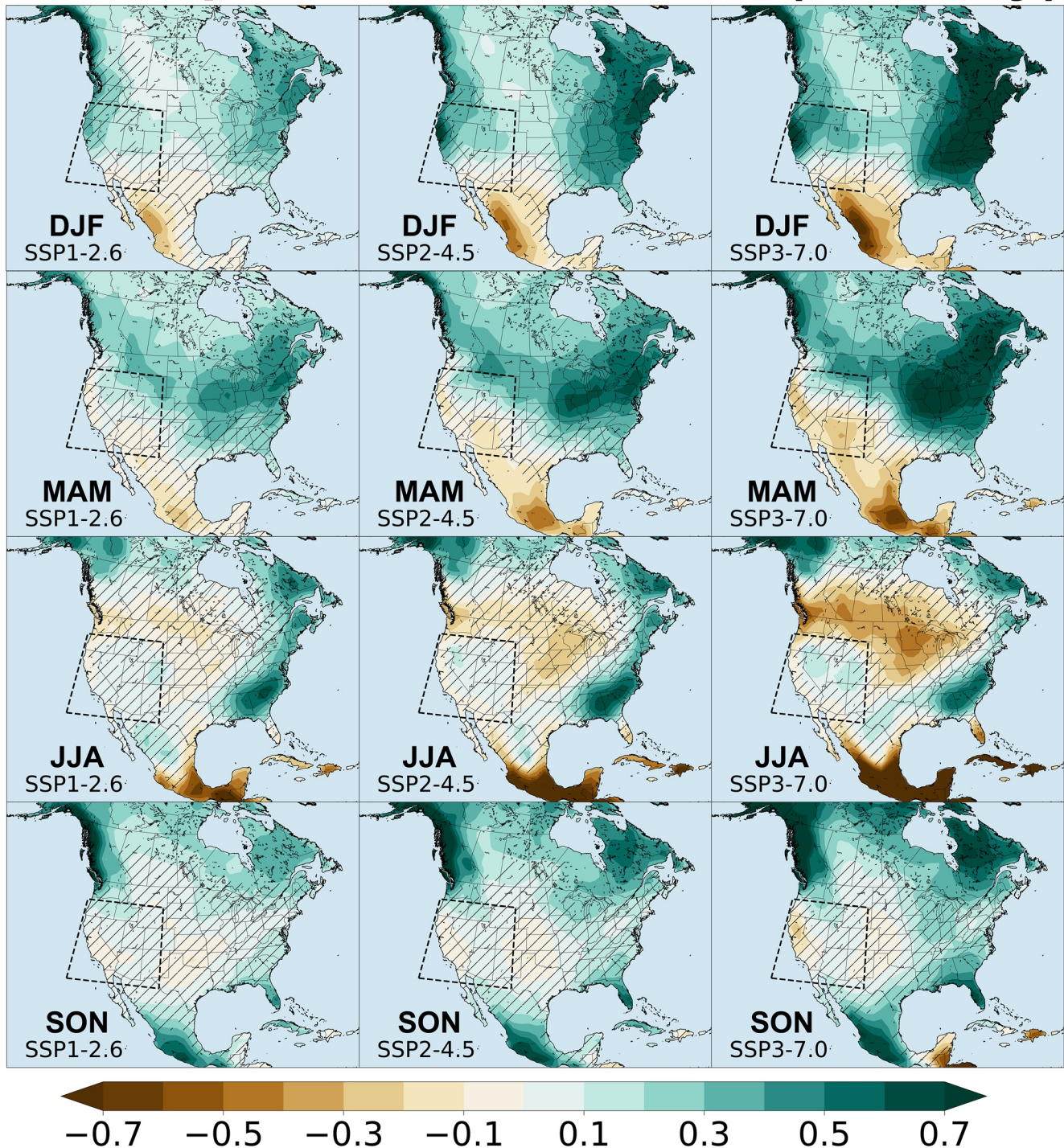
Figure 3. Seasonal changes in precipitation in the multi-model ensemble mean (2071–2100 minus 1971–2000) for each shared socioeconomic pathway for winter (DJF; December-January-February), spring (MAM; March-April-May), summer (JJA; June-July-August), and fall (SON; September-October-November). Hatching indicates regions with non-robust responses (R < 0.80).

ΔVapor Pressure Deficit, 2071-2100 (hPa)
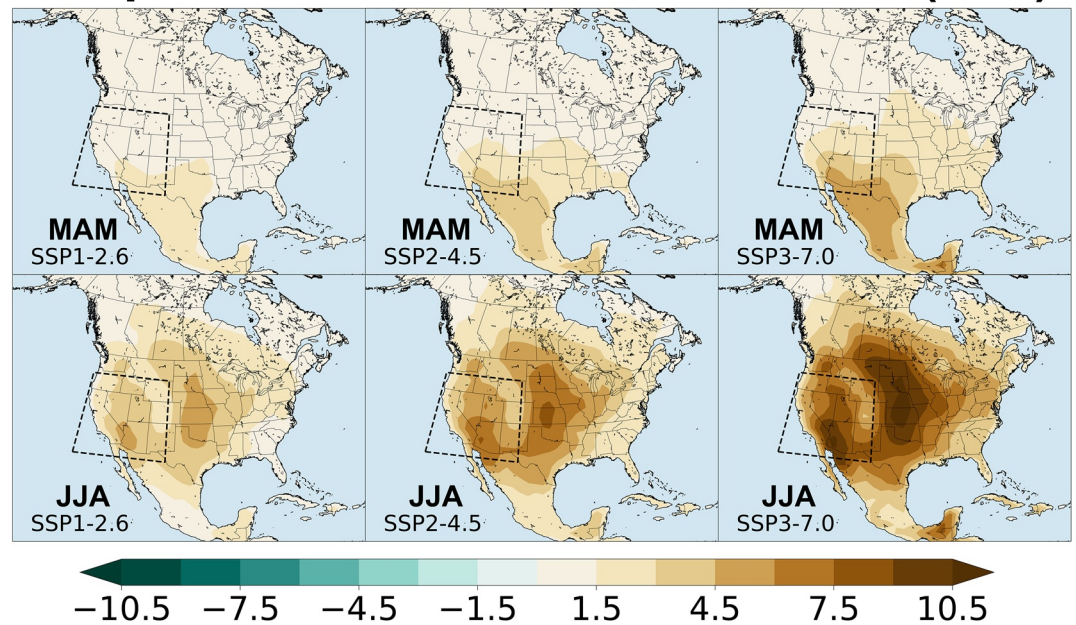
Figure 4. Seasonal changes in vapor pressure deficit in the multi-model ensemble (MME) mean (2071–2100 minus 1971–2000) for each shared socioeconomic pathway for spring (MAM; March-April-May) and summer (JJA; June-July-August). This MME includes all models in Table 1 except BCC-CSM2-MR, which did not provide hurs (surface relative humidity) from the required ensemble members. Hatching indicates regions with non-robust responses (R < 0.80).

over SWNA occur during the spring, are centered mostly over Arizona and New Mexico, and only emerge in the moderate (SSP2-4.5) and high (SSP3-7.0) warming scenarios.

Increasing VPD is the dominant driver of increases in evaporative demand in climate change projections, especially during the warm season. VPD changes are uniform in sign, with robust increases across North America in spring and summer (Figure 4). These robust increases occur as a consequence of the strong dependency of VPD on temperature, which increases everywhere and is one of the most consistent and robust responses of any climate variable in climate model projections (Knutti & Sedlacek, 2013). Increases in VPD are especially large over SWNA, the Pacific Northwest, and the Central Plains, especially during the summer, which likely reflects the exponential response of saturation vapor pressure to temperature.

3.3. Runoff and Soil Moisture

Total runoff decreases across most of western North America in all three scenarios during MAM and JJA, affecting Mexico, SWNA, the Pacific Northwest, and the northern Plains (Figure 5). During MAM in SWNA, runoff declines are strongest and most robust in the southern part of the domain (southern California, Arizona, New Mexico), collocated with the most robust precipitation declines. MAM runoff also declines in more northern parts of SWNA in both seasons, a region with large increases in precipitation during previous months (DJF) and non-robust changes or slight increases in precipitation during MAM. For this part of the SWNA domain, this decline likely reflects increased partitioning of precipitation to rain rather than snow and earlier melting of the snowpack, leading to earlier and lower total runoff during the warm season months. One location in southern Idaho shows strong and robust increases in total runoff during JJA, though it is not clear what, specifically, is driving this hyper-local response. Robust soil moisture drying is much less extensive during spring (Figure 6, top panels), confined primarily to the Pacific coast, Arizona, New Mexico, Texas, and Mexico. Reduced soil drying in spring relative to the warm season is likely a consequence of less snow but increased total precipitation during the cold season, which allows this moisture to infiltrate into the soil and carry over into the spring. Declines in soil moisture are much more intense and widespread in JJA (Figure 6, bottom panels), especially over SWNA. Precipitation changes during this

ΔRunoff (total)
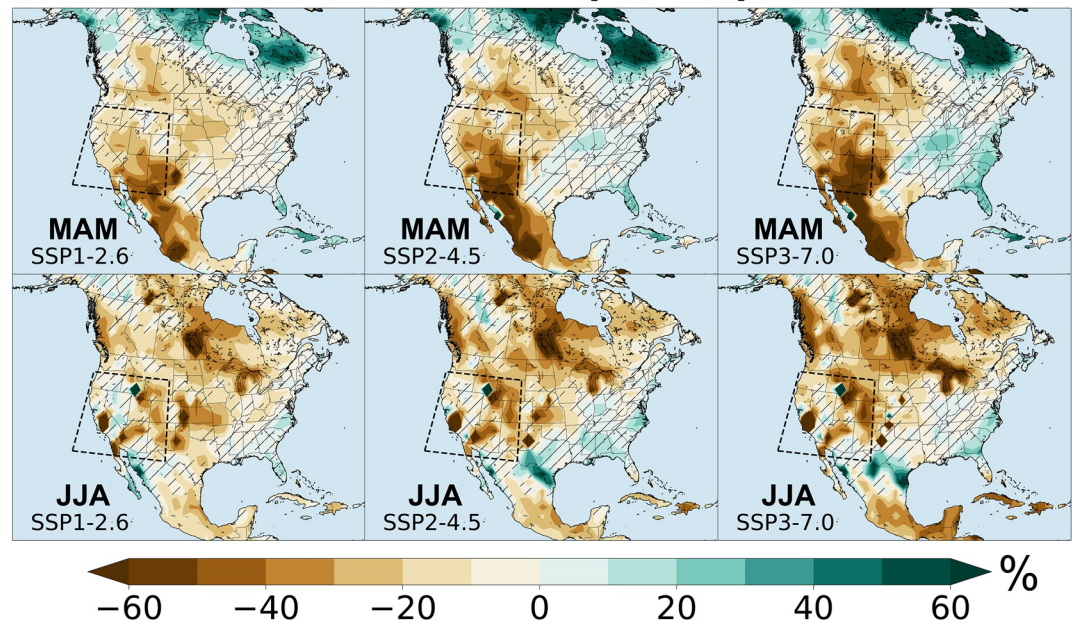
Figure 5. Changes (2071–2100 minus 1971–2000) in the multi-model ensemble (MME) mean total runoff (percent) for the three warming scenarios during spring (MAM; top panels) and summer (JJA; bottom panels). Hatching indicates regions with non-robust responses ($R < 0.80$). The MME used for the total runoff response only includes 15 models (excluding GISS-E2-1-G, MPI-ESM1-2-LR, and NorESM2-MM) because of more limited availability of this model field from our ensemble.

ΔSoil Moisture (0-200 cm)
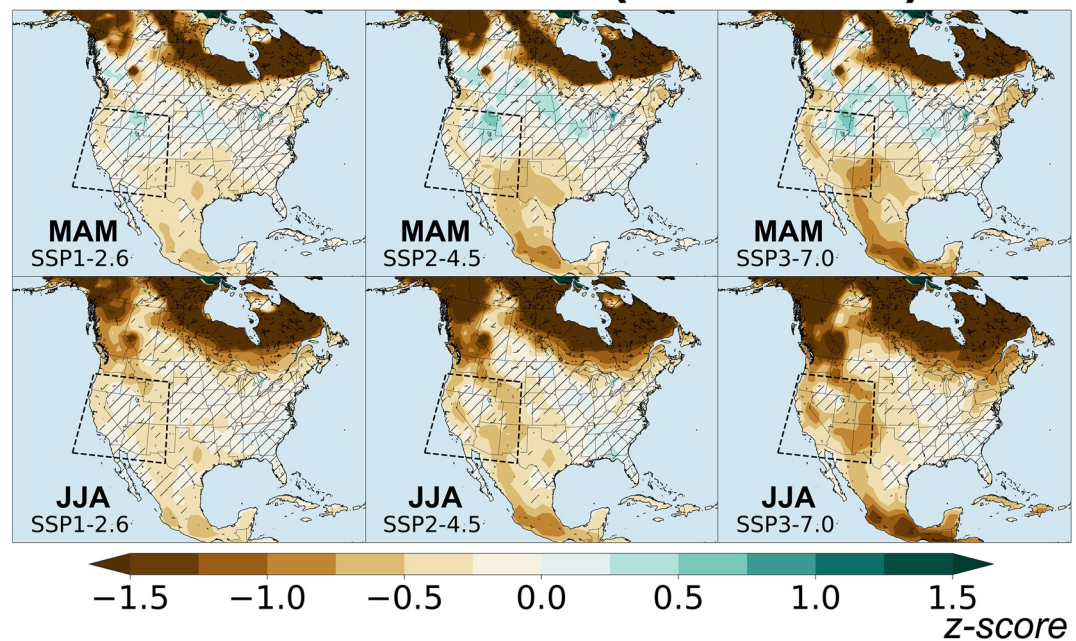
Figure 6. Changes (2071–2100 minus 1971–2000) in the multi-model ensemble mean 200 cm soil moisture (top panels; z-score) for the three warming scenarios during spring (MAM; top panels) and summer (JJA; bottom panels). Hatching indicates regions with non-robust responses ($R < 0.80$).

season are non-robust, though negative precipitation anomalies in MAM likely contribute along with the strong increases in evaporative demand in both of these seasons.

As outlined in the introduction, the expression of the 2002 and 2000–2020 drought in our observational soil moisture index is clearly reflected in other drought metrics, including water resources, vegetation health, and wildfire. Recent studies, however, have highlighted the complexity of vegetation-drought interactions, which can influence how drought is expressed across the hydrologic cycle, especially in climate model projections (Lemordant et al., 2018; Mankin et al., 2017, 2018, 2019; Swann et al., 2016; Swann, 2018). Plant water-use responses to climate and atmospheric carbon dioxide concentrations could theoretically ameliorate surface drying projected by aridity measures (Swann et al., 2016), or even repartition moisture flows to reduce drought risk (Betts et al., 2007). At the same time, however, there is evidence that plant responses to CO_2 do not account for the full gap between aridity measures and prognostic model quantities like soil moisture (Scheff et al., 2021), even as SWNA appears to be one region where the aridity measures and prognostic variables agree (Mankin et al., 2019; Scheff et al., 2021). It is therefore conceivable that, unlike extreme droughts during the 20th century, soil moisture responses in the future may not be indicative of overall declines in surface water availability. To assess whether our soil moisture index adequately represents declines in overall surface water availability in the projections, we compare changes in runoff (Figure 5) and soil moisture (Figure 6) across SWNA. During JJA, robust declines in both quantities occur across most of SWNA in the projections from our CMIP6 MME. This confirms that changes in the soil moisture index that we use to define extreme drought are consistent with overall declines in the surface water resources available to supply societal and ecological demands.

3.4. Soil Moisture Trends and Extreme Drought

Soil moisture time series from the MME show that the drying evident at the end of the 21st century (Figure 6) is part of a long-term trend that begins in the ensemble in the latter part of the twentieth century (Figure 7a). Trend comparisons between the soil moisture reconstruction and individual models in our MME for three different intervals are shown in Figure 7b. The observed drying (negative) trend from 1901–2020 is well captured by the MME, matching closely to the ensemble median trend. Median ensemble drying is larger than observed for the latter half of the twentieth century (1950–2020), though the observed trend still falls within the range simulated by the models. The observed drying from 1950–2020 is relatively weak because SWNA experienced a major drought in the mid-twentieth century at the beginning of this trend estimate (Heim, 2017; Seager et al., 2005). By contrast, no model in the ensemble has an equivalent or larger drying trend than observed for the most recent period (1980–2020). The decades preceding the 2000–2020 drought were some of the wettest in the reconstruction (Williams et al., 2020), and only two other 41-year periods had larger observed drying trends, both during this interval (1978–2018 and 1979–2019).

To investigate if the models can even produce such large magnitude short-term drying trends, we calculated all possible 41-year trends in the ensemble for the available instrumental period (1851–2020). Across the ensemble, 41-year trends of equal or greater magnitude to the observed trend from 1980–2020 occur five times. More generally, the models produce large magnitude trends with a similar frequency to the reconstruction; for example, the fifth percentile trends from the observations and models are −0.03 and −0.04 σ per year, respectively. The models in the ensemble are therefore capable of reproducing extreme short-term drying trends similar to what was observed in recent decades. The mismatch between models and observations for 1980–2020 is thus likely a consequence of how rare such severe drying trends are in both observations and models, and the limited sampling in the model ensemble during this period.

We now evaluate the single- and 21-year drought analogs for the latter part of the 21st century (2071–2100) in our ensemble. In all three SSPs, the distributions of single- and 21-year mean soil moisture anomalies shift towards drier conditions (Figures 8a and 8b) with substantially increased risks of 2002 and 2000–2020 drought analogs (Figures 8c and 8d). For single-year soil moisture, model distributions are unimodal, and the historical simulated distribution matches closely with the reconstruction: conditions equal or drier than 2002 occur in 0.74% of years in our reconstruction and in 0.88% of all years pooled from the instrumental period (1851–2020) from our model ensemble ($n = 3,060$). The risk of these events increases substantially in the SSPs and scales strongly with the forcing. Across all possible years from 2071–2100 pooled from our

Soil Moisture (200 cm)
### *(models and observations)*
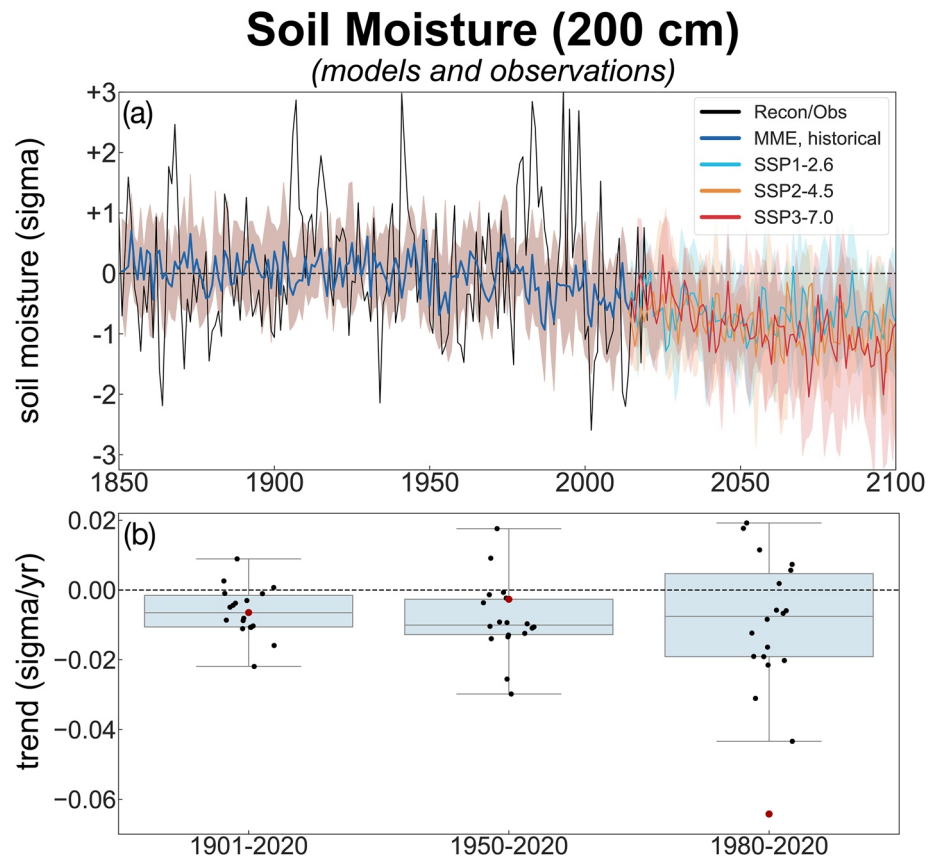
Figure 7. (a) Soil moisture time series for southwestern North America (SWNA) from the reconstruction (solid black lines) and the multi-model ensemble (MME). Solid colored lines are the MME median in each shared socioeconomic pathway (SSP), while the shading indicates the interquartile range across models in the MME. (b) SWNA soil moisture trends for the reconstruction (red dots) and individual models from the MME (black dots) for three historical intervals. Historical simulations in the models end in 2014; for these trend estimates, we therefore extended the time series through 2020 using output from the SSP2-4.5 scenario.

ensemble ($n = 540$), the frequency of these events increases to 8.3% of all years in SSP1-2.6, 14.4% in SSP2-4.5, and 25.9% in SSP3-7.0.

Over the instrumental period, the ensemble simulated 21-year mean soil moisture distributions have an extended dry tail compared to the reconstruction and a higher prevalence of extreme 21-year drought periods. Indeed, 2000–2020 drought analogs, while still exceedingly rare, are much more common in the model historical simulations (4.9% of all years) compared to the reconstruction (0.25% of all years). The 21-year mean soil moisture distributions from the SSPs have a pronounced bimodality that is absent in the single-year soil moisture and a much higher risk for 2000–2020 drought analogs: 47.0% of all years in SSP1-2.6 have a 21-year mean that matches or exceeds 2000–2020, with only slightly higher frequencies in SSP2-4.5 (53.3%) and SSP3-7.0 (53.5%). Only six of the 18 models do not simulate any 2000–2020 drought analogs in any of the SSPs: ACCESS-CM2, GISS-E2-1-G, IPSL-CM6A-LR, KACE-1-0-G, MPI-ESM1-2-HR, and UKESM1-0-LL.

3.5. Drought Responses Across the MME

To investigate the bimodality in the 21-year mean soil moisture response, and the apparent lack of sensitivity of 21-year drought risk to the magnitude of warming, we examined single-year (Figure 9a) and 21-year mean (Figure 9b) soil moisture values for each individual model in our ensemble. As expected, the distribution of single-year soil moisture shifts progressively drier with the magnitude of warming in most models, with the notable exceptions of MPI-ESM1-2-HR and UKESM1-0-LL, where soil moisture increases. For the 21-year mean soil moisture, there is a strong divergence in responses across models. In nine models
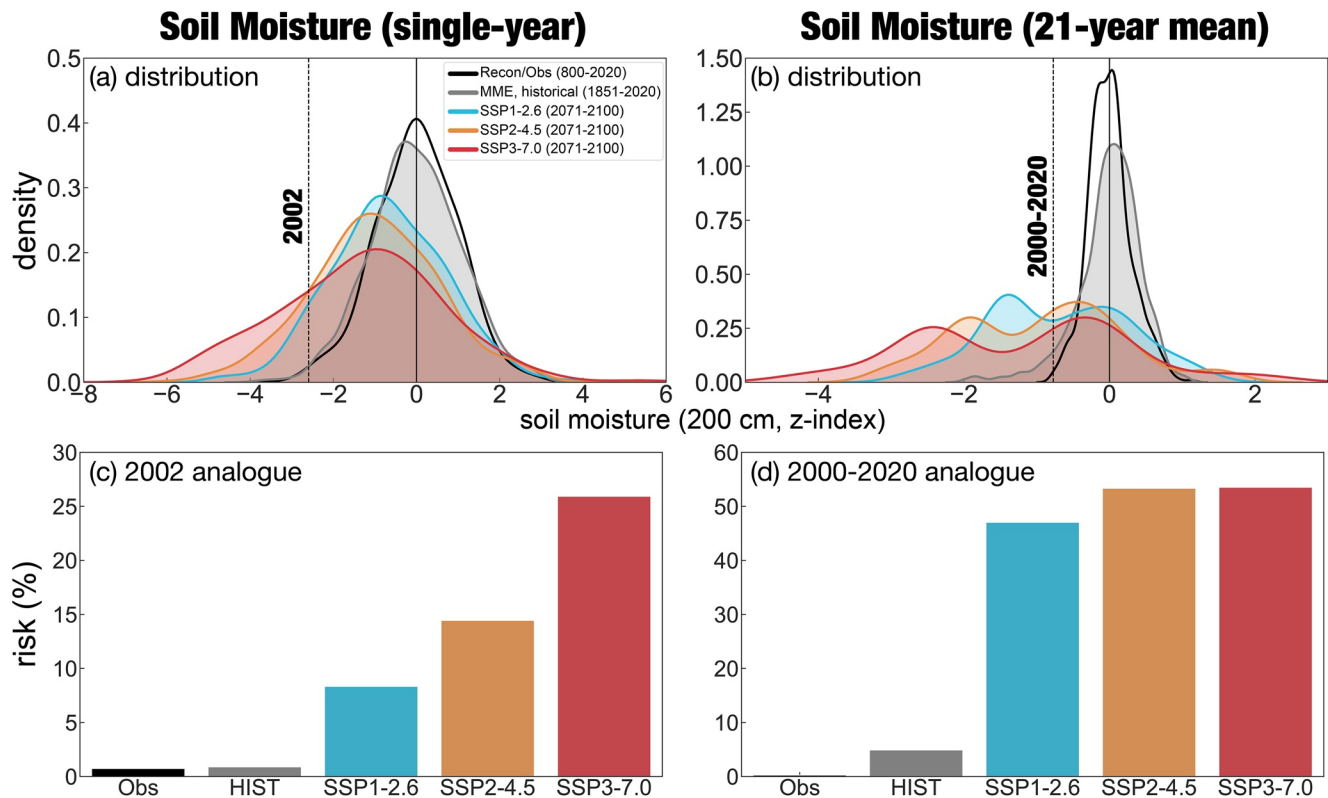
Figure 8. (a), (b) Kernel density plots of single-year and 21-year mean southwestern North America soil moisture from the reconstruction (800–2020), the instrumental period in the simulations (1851–2020), and each shared socioeconomic pathway (SSP) (2071–2100). For the historical MME distributions, output from 1851–2014 is taken from the historical simulations and output from 2015–2020 is taken from SSP2-4.5. The density functions for the models are created by pooling all models and all years together ($n = 3{,}060$ for the historical and $n = 540$ in each SSP). Vertical dashed lines indicate the magnitude of the 2002 and 2000–2020 drought events in the reconstruction. (c), (d) Risk of drought events of equal or greater severity to the 2002 and 2000–2020 drought events, calculated as the fractions of years in the reconstruction or pooled model ensemble equal to or drier than the 2002 and 2000–2020 events in the reconstruction. Risk for 2000–2020 drought analogs in the reconstruction from 800–2020 is exceptionally low (0.25%), highlighting the extreme nature of this event within the paleoclimate and historical record.

(BCC-CSM2-MR, CanESM5, CESM2, CESM2-WACCM, CNRM-CM6-1, CNRM-ESM2-1, EC-Earth3-Veg, MRI-ESM2-0, NorESM2-MM), the median in all three SSPs exceeds the 2000–2020 threshold (Figure 9b, vertical dashed line). We categorize this half of the ensemble as "high-risk," and it is these models that create the drier peak in the full MME 21-year mean soil moisture distributions (Figure 8b). The remaining nine "low-risk" models (ACCESS-ESM1-5, ACCESS-CM2, GISS-E2-1-G, IPSL-CM6A-LR, KACE-1-0-G, MIROC6, MPI-ESM1-2-LR, MPI-ESM1-2-HR, UKESM1-0-LL) have more modest drying or even increased soil moisture, creating the secondary, less dry peak in Figure 8b. This low-risk ensemble includes all six models that do not simulate any 2000–2020 drought analogs in the projections. Because median values from the low-risk models do not cross the 2000–2020 threshold in most SSPs, it is the nine high-risk models mainly driving the increase in 21-year drought risk. Furthermore, because the differences between the high and low-risk models are larger than the differences across SSPs within models, the forcing scenario has little influence on 21-year drought risk in the full MME.

To understand why the response is so different between the high and low-risk models, we compared the climate sensitivities between the model groups and the regional precipitation and temperature responses. Median climate sensitivity in the high-risk models is $4.8\,\mathrm{K}/2 \times CO_2$, moderately higher than for the low-risk models, which have a median climate sensitivity of $3.9\,\mathrm{K}/2 \times CO_2$. The range of climate sensitivities within the two model groups is comparable across the two, however: 2.5–$5.6\,\mathrm{K}/2 \times CO_2$ in the high-risk and 2.6–$5.3\,\mathrm{K}/2 \times CO_2$ for the low-risk. Additionally, we observe that even models with nearly the same sensitivities across the two groups can have dramatically different soil moisture responses over the SWNA. Contrast, for example, the strong drying in BCC-CSM2-MR with the much more muted response in GISS-E2-1-G
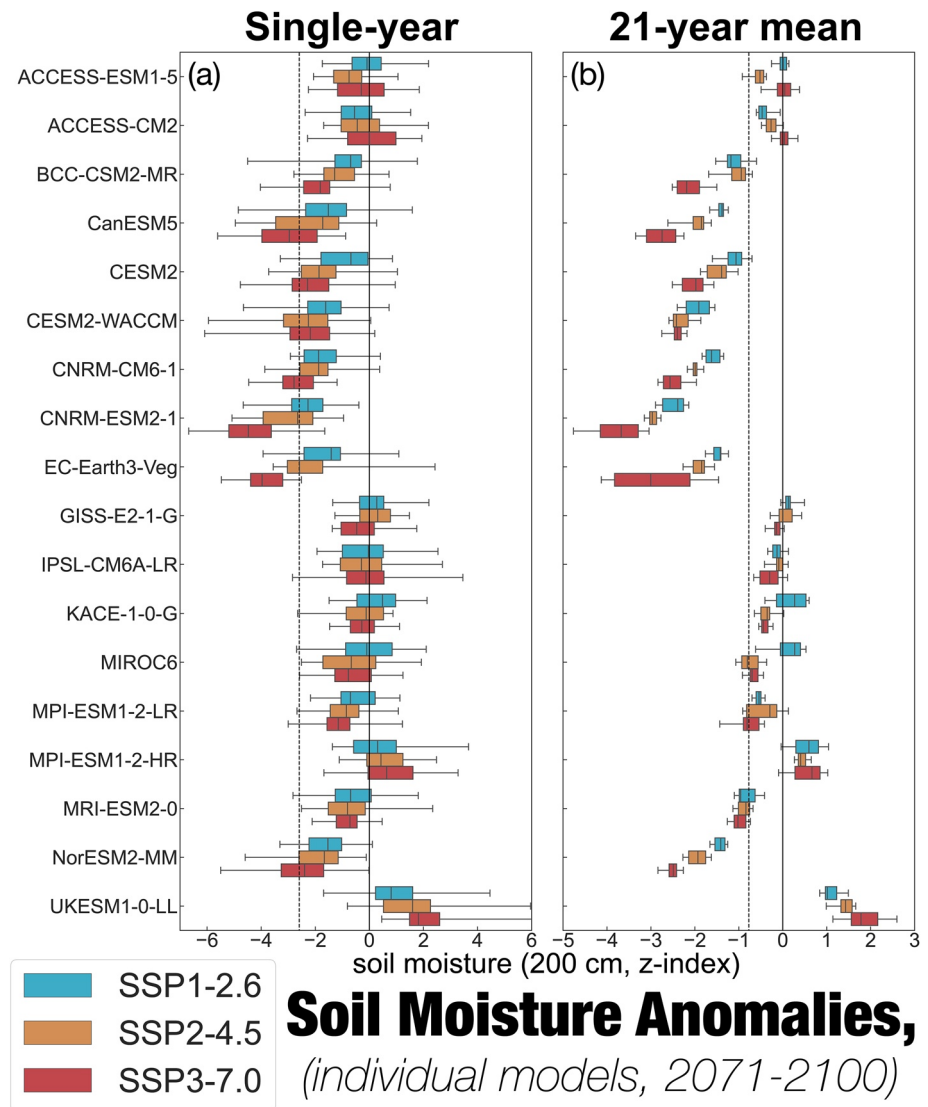
Figure 9. Single- (a) and 21-year mean (b) soil moisture anomalies in southwestern North America from the shared socioeconomic pathways for individual models in our ensemble. Each boxplot encompasses the full range of values ($n = 30$) for the different models from 2071–2100. Dashed lines indicate the values of the 2002 and 2000–2020 droughts in the reconstruction.

(Figure 9), despite the fact that both models have approximate climate sensitivities of 3.0 K/2 × CO_2. It therefore seems unlikely that climate sensitivity specifically can explain the differences across these two sets of models.

Declines in spring precipitation are larger and more robust in the ensemble mean of the high-risk models compared to the low-risk models, especially across the southern half of SWNA (Figure 10). At the same time, the low-risk models show a modest increase in precipitation during the summer, a signal that is absent in the high-risk models. Together, these differential precipitation responses would amplify soil moisture drying in the high-risk models and reduce it in the low-risk models, likely accounting for the majority of the difference in soil moisture drought between these two model groups. Warming during spring and summer is also slightly higher in SWNA over Arizona and New Mexico in the high-risk models (not shown), the same area with the amplified declines in spring precipitation. While this slightly enhanced warming could amplify soil moisture losses by increasing evaporative demand, this model response could instead be a consequence of the enhanced soil moisture drying in the high-risk models (e.g., an increased Bowen ratio).
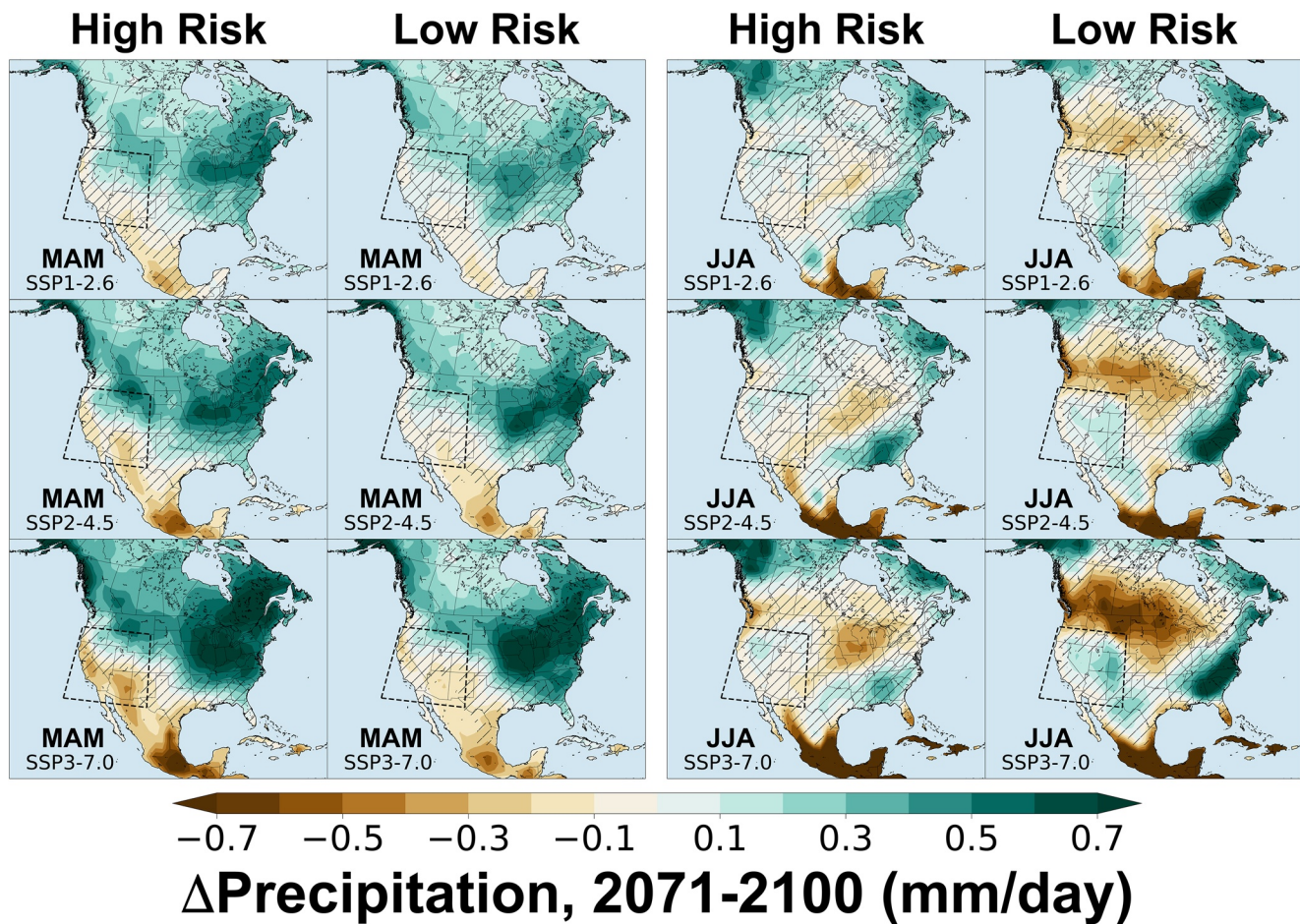
Figure 10. Ensemble mean spring and summer season changes (2071–2100 minus 1971–2000) in precipitation (mm day^{-1}) for the 9 "high-risk" models (BCC-CSM2-MR, CanESM5, CESM2, CESM2-WACCM, CNRM-CM6-1, CNRM-ESM2-1, EC-Earth3-Veg, MRI-ESM2-0, NorESM2-MM) and 9 "low-risk" (ACCESS-ESM1-5, ACCESS-CM2, GISS-E2-1-G, IPSL-CM6A-LR, KACE-1-0-G, MIROC6, MPI-ESM1-2-LR, MPI-ESM1-2-HR, UKESM1-0-LL) models in our CMIP6 ensemble. Hatching indicates regions with non-robust responses ($R < 0.80$).

Even if warming mitigation offers little capacity for reducing the occurrence of 2000–2020 drought analogs, there may still be mitigation benefits from reducing the intensity or severity of these events. To test this, we sampled single-year soil moisture from all 2000–2020 drought analogs across our full 18-member MME. Consistent with our previous analyses (Figure 8a), distributions of single-year soil moisture during these events are unimodal and shift progressively drier with increased warming (Figure 11a). Additionally, the risk of 2002 single-year drought analogs during these 21-year events scales strongly with warming (Figure 11b): 18.1% (SSP1-2.6), 24.3% (SSP2-4.5), and 37.2% (SSP3-7.0). This demonstrates that, while mitigation may have little effect on the occurrence of droughts at least as severe as the 2000–2020 analog, it would still have large benefits for reducing the overall severity of these multi-decadal droughts and the risk of the most extreme single-year droughts during these events.

4. Discussion & Conclusions

As in the previous generation of climate models (Cook et al., 2015; Cook et al., 2018), the latest projections from CMIP6 demonstrate that future warming will likely increase soil moisture drought risk across SWNA to levels far outside the envelope of natural variability from the last millennium. Here, we analyzed model-projected responses to anthropogenic climate change of both single- and 21-year soil moisture droughts, focusing on analogs of recent events (2002 and 2000–2020) in SWNA that had large, established impacts on people and ecosystems. While mean-state drying and the risk of extreme single-year soil moisture drought
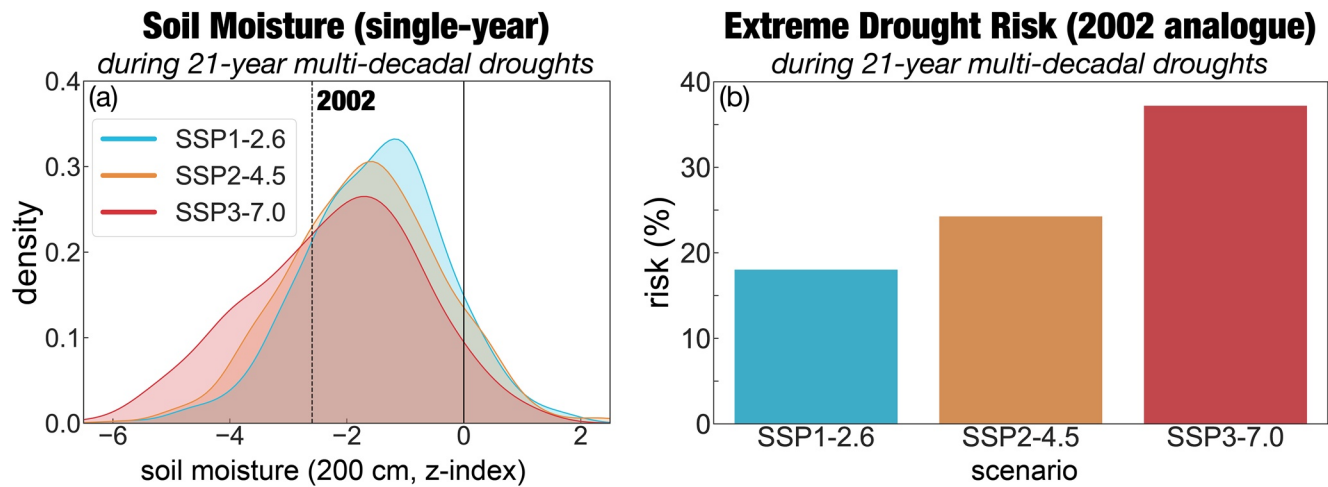
Figure 11. (a) Kernel density plot of single-year southwestern North America soil moisture sampled from three socioeconomic pathways during 21-year mean drought events matching or exceeding the 2000–2020 analog. For these analyses, the maximum number of years available from the ensemble is larger ($n = 900$), as 21-year trailing mean values earlier in our 2071–2100 period incorporate years before this interval begins. Further, because the occurrence of these long-term droughts varies across models and scenarios, the sample size in these distributions is different for each SSP: $n = 437$ (SSP1-2.6), $n = 539$ (SSP2-4.5), and $n = 521$ (SSP3-7.0). (b) Risk of single-year drought events of equal or greater magnitude to 2002 during the 21-year droughts, calculated as the fractions of years from (a) equal to or drier than the 2002 magnitude in the reconstruction.

events scales strongly with the magnitude of warming, even the most conservative warming scenario (SSP1-2.6, +2.1 K) results in an approximate 50% likelihood of a 21-year drought at least as severe as 2000–2020 by the end of the 21st century. This strong response of long-term droughts in the models is a consequence of large spring season precipitation declines in half the models in our ensemble, where the median soil moisture response exceeds the dryness of 2000–2020 in all warming scenarios. However, though warming mitigation may not be effective at reducing the likelihood of occurrence of droughts similar to 2000–2020, there are clearly strong benefits for alleviating the overall magnitude of drying, the intensity of these droughts, and the risk of extreme single-year droughts similar to 2002.

Our results from the latest generation of climate models in CMIP6 are broadly similar to earlier studies (Ault et al., 2016; Cook et al., 2015; Overpeck & Udall, 2020; Spinoni et al., 2020; Zhao et al., 2020), which also found large projected declines in warm season soil moisture and runoff over this region of North America in the twenty-first century. In the one study that specifically investigated climate mitigation effects on multi-decadal droughts, Ault et al. (2016) found that the risk of these events was strongly reduced with climate mitigation, an apparently contrary result to our own findings. However, Ault et al. (2016) focused on events that were more persistent (35-year) and modest in severity (-0.5σ) than the shorter and more severe 2000–2020 event we used as an analog for our analyses. Ault et al. (2016) also found that the mitigation benefits were primarily a consequence of differences in the magnitude of warming across the SSPs, while in our CMIP6 ensemble 21-year drought risk was most strongly related to precipitation differences across models and not temperature or precipitation differences across scenarios. Divergent results across these two studies are therefore likely due, at least in part, to differences in both how drought was defined and climate in the models and scenarios within the different ensembles.

Our analyses clearly highlight the importance of precipitation uncertainties in climate change projections of drought. As in the last generation of climate models (Knutti & Sedlacek, 2013), precipitation in the CMIP6 projections is one of the most uncertain and least robust responses in the models (Cook et al., 2020; Ukkola et al., 2020), especially in mid-latitude regions. This is clear in our ensemble, where much of the drying and especially the increase in 21-year drought risk is forced by larger precipitation declines in the models comprising the high-risk half of our ensemble. At the same time, drought risk is ameliorated in the low-risk models because these show robust precipitation increases during the summer. Although large and robust spring precipitation declines for SWNA are expected (Ting et al., 2018), improving confidence in drought projections in this, and other regions, would still strongly benefit from better constraining the magnitude of these precipitation responses. While not detailed here, there are also major uncertainties for surface

drought connected to treatments of the land surface and vegetation processes within the models, which can act to ameliorate (Swann, 2018) or amplify (Mankin et al., 2019) soil moisture and runoff droughts. Within our ensemble, projected soil moisture declines during JJA are also associated with reductions in total runoff over SWNA, indicating that, in aggregate, vegetation processes are not sufficient to counteract surface drying forced by changes in precipitation and evaporative demand.

As of spring 2021, the ongoing persistent drought that began in 2000 is continuing to have large impacts across SWNA (Freedman & Dormido, 2021; National Drought Mitigation Center, 2021), a herald for what may be a much drier future in the region with continued warming. As a consequence of its severity and persistence, this drought has motivated substantial action among managers, regional governments, stakeholders, and private investors across the western US to more aggressively and proactively address water resource issues in the face of declining availability and increased demand (Howe, 2021). Results from our analyses demonstrate the clear value of warming mitigation for reducing drought severity and risk in SWNA. Under even the lowest warming scenario, however, increases in drought severity and risk are likely by the end of the 21st century. Building a resilient future in the region will therefore require additional and ongoing adaptation measures and policies to manage water resources in a world that will be warmer and drier compared to the past.

Data Availability Statement

The updated SWNA regional average reconstruction we use is available from https://www.ldeo.columbia.edu/~williams/NA_climate/SWNA_SMf_recon_update/20201201/. HadCRUT5 data available from https://crudata.uea.ac.uk/cru/data/temperature/. CMIP6 data available from https://esgf-node.llnl.gov/search/cmip6/.

References

Abatzoglou, J. T., & Williams, A. P. (2016). Impact of anthropogenic climate change on wildfire across western US forests. *Proceedings of the National Academy of Sciences*, *113*(42), 11770–11775. https://doi.org/10.1073/pnas.1607171113

Anderegg, L. D. L., Anderegg, W. R. L., Abatzoglou, J., Hausladen, A. M., & Berry, J. A. (2013). Drought characteristics' role in widespread aspen forest mortality across Colorado, USA. *Global Change Biology*, *19*(5), 1526–1537. https://doi.org/10.1111/gcb.12146

Ault, T. R. (2020). On the essentials of drought in a changing climate. *Science*, *368*(6488), 256–260. https://doi.org/10.1126/science.aaz5492

Ault, T. R., Mankin, J. S., Cook, B. I., & Smerdon, J. E. (2016). Relative impacts of mitigation, temperature, and precipitation on 21st-century megadrought risk in the American Southwest. *Science Advances*, *2*(10), e1600873. https://doi.org/10.1126/sciadv.1600873

Bentsen, M., Oliviè, D. J. L., Seland, y., Toniazzo, T., Gjermundsen, A., Graff, L. S., & Schulz, M. (2019a). *NCC NorESM2-MM Model Output Prepared for CMIP6 CMIP*. Earth System Grid Federation. https://doi.org/10.22033/ESGF/CMIP6.506

Bentsen, M., Oliviè, D. J. L., Seland, y., Toniazzo, T., Gjermundsen, A., Graff, L. S., & Schulz, M. (2019b). *NCC NorESM2-MM model output prepared for CMIP6 ScenarioMIP*. Earth System Grid Federation. https://doi.org/10.22033/ESGF/CMIP6.608

Berg, N., & Hall, A. (2017). Anthropogenic warming impacts on California snowpack during drought. *Geophysical Research Letters*, *44*(5), 2511–2518. https://doi.org/10.1002/2016GL072104

Betts, R. A., Boucher, O., Collins, M., Cox, P. M., Falloon, P. D., Gedney, N., et al. (2007). Projected increase in continental runoff due to plant responses to increasing carbon dioxide. *Nature*, *448*, 1037–1041. https://doi.org/10.1038/nature06045

Boucher, O., Denvil, S., Caubel, A., & Foujols, M. A. (2018). *IPSL IPSL-CM6A-LR model output prepared for CMIP6 CMIP*. https://doi.org/10.22033/ESGF/CMIP6.1534

Boucher, O., Denvil, S., Caubel, A., & Foujols, M. A. (2019). *IPSL IPSL-CM6A-LR model output prepared for CMIP6 ScenarioMIP*. Earth System Grid Federation. https://doi.org/10.22033/ESGF/CMIP6.1532

Byun, Y.-H., Lim, Y.-J., Shim, S., Sung, H. M., Sun, M., Kim, J., & Moon, H. (2019). *NIMS-KMA KACE1.0-G model output prepared for CMIP6 ScenarioMIP*. Earth System Grid Federation. https://doi.org/10.22033/ESGF/CMIP6.2242

Byun, Y.-H., Lim, Y.-J., Sung, H. M., Kim, J., Sun, M., & Kim, B.-H. (2019). *NIMS-KMA KACE1.0-G model output prepared for CMIP6 CMIP*. Earth System Grid Federation. https://doi.org/10.22033/ESGF/CMIP6.2241

Cook, B. I., Ault, T. R., & Smerdon, J. E. (2015). Unprecedented 21st century drought risk in the American Southwest and Central Plains. *Science Advances*, *1*(1), e1400082. https://doi.org/10.1126/sciadv.1400082

Cook, B. I., Cook, E. R., Smerdon, J. E., Seager, R., Williams, A. P., Coats, S., et al. (2016). North American megadroughts in the common era: Reconstructions and simulations. *Wiley Interdisciplinary Reviews: Climate Change*, *7*, 411–432. https://doi.org/10.1002/wcc.394

Cook, B. I., Mankin, J. S., & Anchukaitis, K. J. (2018). Climate change and drought: From past to future. *Current Climate Change Reports*, *4*(2), 164–179. https://doi.org/10.1007/s40641-018-0093-2

Cook, B. I., Mankin, J. S., Marvel, K., Williams, A. P., Smerdon, J. E., & Anchukaitis, K. (2020). Twenty-first century drought projections in the CMIP6 forcing scenarios. *Earth's Future*, *8*(6), e2019EF001461. https://doi.org/10.1029/2019EF001461

Cook, B. I., Seager, R., Williams, A. P., Puma, M. J., McDermid, S., Kelley, M., & Nazarenko, L. (2019). Climate change amplification of natural drought variability: The historic mid-twentieth-century North American drought in a warmer world. *Journal of Climate*, *32*(17), 5417–5436. https://doi.org/10.1175/JCLI-D-18-0832.1

Cook, B. I., Smerdon, J. E., Seager, R., & Coats, S. (2014). Global Warming and 21st century drying. *Climate Dynamics*, *43*(9–10), 2607–2627. https://doi.org/10.1007/s00382-014-2075-y

Cooley, H., Donnelly, K., Phurisamban, R., & Subramanian, M. (2015). *Impacts of California's ongoing drought: Agriculture*. Pacific Institute.

Danabasoglu, G. (2019a). *NCAR CESM2 model output prepared for CMIP6 CMIP historical*. https://doi.org/10.22033/ESGF/CMIP6.7627

Danabasoglu, G. (2019b). *NCAR CESM2-WACCM model output prepared for CMIP6 CMIP*. Earth System Grid Federation. https://doi.org/10.22033/ESGF/CMIP6.10024

Danabasoglu, G. (2019c). *NCAR CESM2-WACCM model output prepared for CMIP6 ScenarioMIP*. Earth System Grid Federation. https://doi.org/10.22033/ESGF/CMIP6.10026

Delworth, T. L., Zeng, F., Rosati, A., Vecchi, G. A., & Wittenberg, A. T. (2015). A Link between the hiatus in global warming and North American drought. *Journal of Climate*, *28*(9), 3834–3845. https://doi.org/10.1175/JCLI-D-14-00616.1

Diersen, M. A. (2003). Farm Sector Recovery Following the 2002 drought. 444. Economics Commentator.

Dix, M., Bi, D., Dobrohotoff, P., Fiedler, R., Harman, I., Law, R., & Yang, R. (2019a). *CSIRO-ARCCSS ACCESS-CM2 model output prepared for CMIP6 CMIP historical*. Earth System Grid Federation. https://doi.org/10.22033/ESGF/CMIP6.4271

Dix, M., Bi, D., Dobrohotoff, P., Fiedler, R., Harman, I., Law, R., & Yang, R. (2019b). *CSIRO-ARCCSS ACCESS-CM2 model output prepared for CMIP6 ScenarioMIP ssp126*. Earth System Grid Federation. https://doi.org/10.22033/ESGF/CMIP6.4319

EC-Earth Consortium (EC-Earth). (2019a). *EC-Earth-Consortium EC-Earth3-Veg model output prepared for CMIP6 CMIP*. Earth System Grid Federation. https://doi.org/10.22033/ESGF/CMIP6.642

EC-Earth Consortium (EC-Earth). (2019b). *EC-Earth-Consortium EC-Earth3-Veg model output prepared for CMIP6 ScenarioMIP*. Earth System Grid Federation. https://doi.org/10.22033/ESGF/CMIP6.727

Eyring, V., Bony, S., Meehl, G. A., Senior, C., Stevens, B., Stouffer, R. J., & Taylor, K. E. (2016). Overview of the coupled model intercomparison project phase 6 (cmip6) experimental design and organisation. *Geoscientific Model Development Discussions*, *8*, 1937–1958. https://doi.org/10.5194/gmdd-8-10539-2015

Faunt, C. C., Sneed, M., Traum, J., & Brandt, J. T. (2016). Water availability and land subsidence in the Central Valley, California, USA. *Hydrogeology Journal*, *24*(3), 675–684. https://doi.org/10.1007/s10040-015-1339-x

Fettig, C. J., Mortenson, L. A., Bulaon, B. M., & Foulk, P. B. (2019). Tree mortality following drought in the central and southern Sierra Nevada, California, US. *Forest Ecology and Management*, *432*, 164–178. https://doi.org/10.1016/j.foreco.2018.09.006

Freedman, A., & Dormido, H. (2021). *Drought is the sleeper weather story you'll hear more about in 2021*. Washington Post. Retrieved from https://www.washingtonpost.com/weather/2021/01/07/drought-expands-north-america/?arc404=true

Ganey, J. L., & Vojta, S. C. (2011). Tree mortality in drought-stressed mixed-conifer and ponderosa pine forests, Arizona, USA. *Forest Ecology and Management*, *261*(1), 162–168. https://doi.org/10.1016/j.foreco.2010.09.048

Gergel, D. R., Nijssen, B., Abatzoglou, J. T., Lettenmaier, D. P., & Stumbaugh, M. R. (2017). Effects of climate change on snowpack and fire potential in the western USA. *Climatic Change*, *141*(2), 287–299. https://doi.org/10.1007/s10584-017-1899-y

Good, P., Sellar, A., Tang, Y., Rumbold, S., Ellis, R., Kelley, D., & Walton, J. (2019). *MOHC UKESM1.0-LL model output prepared for CMIP6 ScenarioMIP*. Earth System Grid Federation. https://doi.org/10.22033/ESGF/CMIP6.1567

Harpold, A. A., Molotch, N. P., Musselman, K. N., Bales, R. C., Kirchner, P. B., Litvak, M., & Brooks, P. D. (2015). Soil moisture response to snowmelt timing in mixed-conifer subalpine forests. *Hydrological Processes*, *29*(12), 2782–2798. https://doi.org/10.1002/hyp.10400

Heim, R. R. (2017). A comparison of the early twenty-first century drought in the United States to the 1930s and 1950s drought episodes. *Bulletin of the American Meteorological Society*, *98*(12), 2579–2592. https://doi.org/10.1175/BAMS-D-16-0080.1

Howe, B. R. (2021). *Wall street eyes billions in the Colorado's water*. New York Times. Retrieved from https://www.nytimes.com/2021/01/03/business/colorado-river-water-rights.html

Jungclaus, J., Bittner, M., Wieners, K.-H., Wachsmann, F., Schupfner, M., Legutke, S., & Roeckner, E. (2019). *MPI-M MPIESM1.2-HR model output prepared for CMIP6 CMIP*. Earth System Grid Federation. https://doi.org/10.22033/ESGF/CMIP6.741

Knutti, R., & Sedlacek, J. (2013). Robustness and uncertainties in the new CMIP5 climate model projections. *Nature Climate Change*, *3*(4), 369–373. https://doi.org/10.1038/nclimate1716

Krasting, J. P., Broccoli, A. J., Dixon, K. W., & Lanzante, J. R. (2013). Future changes in Northern hemisphere snowfall. *Journal of Climate*, *26*(20), 7813–7828. https://doi.org/10.1175/JCLI-D-12-00832.1

Lehner, F., Deser, C., Simpson, I. R., & Terray, L. (2018). Attributing the U.S. Southwest's recent shift into drier conditions. *Geophysical Research Letters*, *45*(12), 6251–6261. https://doi.org/10.1029/2018GL078312

Lemordant, L., Gentine, P., Swann, A. S., Cook, B. I., & Scheff, J. (2018). Critical impact of vegetation physiology on the continental hydrologic cycle in response to increasing CO_2. *Proceedings of the National Academy of Sciences*, *115*(16), 4093, 4098. https://doi.org/10.1073/pnas.1720712115

Li, D., Wrzesien, M. L., Durand, M., Adam, J., & Lettenmaier, D. P. (2017). How much runoff originates as snow in the western United States, and how will that change in the future? *Geophysical Research Letters*, *44*(12), 6163–6172. https://doi.org/10.1002/2017GL073551

Mankin, J. S., & Diffenbaugh, N. S. (2015). Influence of temperature and precipitation variability on near-term snow trends. *Climate Dynamics*, *45*(3), 1099–1116. https://doi.org/10.1007/s00382-014-2357-4

Mankin, J. S., Lehner, F., Coats, S., & McKinnon, K. A. (2020). The value of initial condition large ensembles to robust adaptation decision-making. *Earth's Future*, *8*(10), e2012EF001610. https://doi.org/10.1029/2020EF001610

Mankin, J. S., Seager, R., Smerdon, J. E., Cook, B. I., & Williams, A. P. (2019). Mid-latitude freshwater availability reduced by projected vegetation responses to climate change. *Nature Geoscience*, *12*, 983–988. https://doi.org/10.1038/s41561-019-0480-x

Mankin, J. S., Seager, R., Smerdon, J. E., Cook, B. I., Williams, A. P., & Horton, R. (2018). Blue water tradeoffs with vegetation in a CO_2 enriched climate. *Geophysical Research Letters*, *45*, 3115–3125. https://doi.org/10.1002/2018GL077051

Mankin, J. S., Smerdon, J. E., Cook, B. I., Williams, A. P., & Seager, R. (2017). The curious case of projected twenty-first-century drying but greening in the American West. *Journal of Climate*, *30*(21), 8689–8710. https://doi.org/10.1175/JCLI-D-17-0213.1

Mankin, J. S., Viviroli, D., Singh, D., Hoekstra, A. Y., & Diffenbaugh, N. S. (2015). The potential for snow to supply human water demand in the present and future. *Environmental Research Letters*, *10*(11), 114016. https://doi.org/10.1088/1748-9326/10/11/114016

Marlier, M. E., Xiao, M., Engel, R., Livneh, B., Abatzoglou, J. T., & Lettenmaier, D. P. (2017). The 2015 drought in Washington State: A harbinger of things to come? *Environmental Research Letters*, *12*(11), 114008. https://doi.org/10.1088/1748-9326/aa8fde

Marvel, K., Cook, B. I., Bonfils, C., Smerdon, J. E., Williams, A. P., & Liu, H. (in review). *Projected changes to hydroclimate seasonality in the 1 continental United States*. Earth's Future.

McCabe, G. J., Wolock, D. M., Pederson, G. T., Woodhouse, C. A., & McAfee, S. (2017). Evidence that recent warming is reducing upper Colorado river flows. *Earth Interactions*, *21*, 1–14. https://doi.org/10.1175/EI-D-17-0007.1

Meehl, G. A., Senior, C. A., Eyring, V., Flato, G., Lamarque, J.-F., Stouffer, R. J., et al. (2020). Context for interpreting equilibrium climate sensitivity and transient climate response from the CMIP6 Earth system models. *Science Advances*, *6*(26), eaba1981. https://doi.org/10.1126/sciadv.aba1981

Morice, C. P., Kennedy, J. J., Rayner, N. A., Winn, J. P., Hogan, E., Killick, R. E., et al. (2020). An updated assessment of near-surface temperature change from 1850: The HadCRUT5 dataset. *Journal of Geophysical Research: Atmospheres*, *126*(3), e2019JD032361. https://doi.org/10.1029/2019JD032361

Mote, P. W., Li, S., Lettenmaier, D. P., Xiao, M., & Engel, R. (2018). Dramatic declines in snowpack in the western US. *npj Climate and Atmospheric Science*, *1*(1), 2. https://doi.org/10.1038/s41612-018-0012-1

Mote, P. W., Rupp, D. E., Li, S., Sharp, D. J., Otto, F., Uhe, P. F., et al. (2016). Perspectives on the causes of exceptionally low 2015 snowpack in the western United States. *Geophysical Research Letters*, *10*, 980–1010. https://doi.org/10.1002/2016GL069965

Musselman, K. N., Addor, N., Vano, J. A., & Molotch, N. P. (2021). Winter melt trends portend widespread declines in snow water resources. *Nature Climate Change*, (Vol. *11*, pp. 418–424). https://doi.org/10.1038/s41558-021-01014-9

NASA Goddard Institute for Space Studies (NASA/GISS). (2018). *NASA-GISS GISS-E2.1G model output prepared for CMIP6 CMIP*. Earth System Grid Federation. https://doi.org/10.22033/ESGF/CMIP6.1400

NASA Goddard Institute for Space Studies (NASA/GISS). (2020). *NASA-GISS GISS-E2.1G model output prepared for CMIP6 ScenarioMIP*. Earth System Grid Federation. https://doi.org/10.22033/ESGF/CMIP6.2074

National Drought Mitigation Center. (2021). *U.S. Drought monitor, April 20, 2021*. Retrieved from https://droughtmonitor.unl.edu/data/pdf/20210420/20210420_usdm.pdf

O'Neill, B. C., Tebaldi, C., van Vuuren, D. P., Eyring, V., Friedlingstein, P., Hurtt, G., et al. (2016). The Scenario model intercomparison project (ScenarioMIP) for CMIP6. *Geoscientific Model Development*, *9*(9), 3461–3482. https://doi.org/10.5194/gmd-9-3461-2016

Overpeck, J. T., & Udall, B. (2020). Climate change and the aridification of North America. *Proceedings of the National Academy of Sciences*, *117*(22), 11856–11858. https://doi.org/10.1073/pnas.2006323117

Scheff, J., & Frierson, D. M. W. (2013). Scaling potential evapotranspiration with greenhouse warming. *Journal of Climate*, *27*, 1539–1558. https://doi.org/10.1175/JCLI-D-13-00233.1

Scheff, J., Mankin, J. S., Coats, S., & Liu, H. (2021). CO_2-plant effects do not account for the gap between dryness indices and projected dryness impacts in CMIP6 or CMIP5. *Environmental Research Letters*, *16*, 034018. https://doi.org/10.1088/1748-9326/abd8fd

Schupfner, M., Wieners, K.-H., Wachsmann, F., Steger, C., Bittner, M., Jungclaus, J., et al. (2019). *DKRZ MPI-ESM1.2-HR model output prepared for CMIP6 ScenarioMIP*. Earth System Grid Federation. https://doi.org/10.22033/ESGF/CMIP6.2450

Schwalm, C. R., Williams, C. A., Schaefer, K., Baldocchi, D., Black, T. A., Goldstein, A. H., et al.(2012). Reduction in carbon uptake during turn of the century drought in western North America. *Nature Geoscience*, *5*(8), 551–556. https://doi.org/10.1038/ngeo1529

Seager, R. (2007). The turn of the century North American drought: Global context, dynamics, and past analogs*. *Journal of Climate*, *20*(22), 5527–5552. https://doi.org/10.1175/2007JCLI1529.1

Seager, R., Kushnir, Y., Herweijer, C., Naik, N., & Velez, J. (2005). Modeling of tropical forcing of persistent droughts and pluvials over western North America: 1856–2000. *Journal of Climate*, *18*(19), 4065–4088. https://doi.org/10.1175/JCLI3522.1

Seferian, R. (2018). *CNRM-CERFACS CNRM-ESM2-1 model output prepared for CMIP6 CMIP*. https://doi.org/10.22033/ESGF/CMIP6.1391

Seferian, R. (2019). *CNRM-CERFACS CNRM-ESM2-1 model output prepared for CMIP6 ScenarioMIP*. Earth System Grid Federation. https://doi.org/10.22033/ESGF/CMIP6.1395

Shi, H. X., & Wang, C. H. (2015). Projected 21st century changes in snow water equivalent over Northern Hemisphere landmasses from the CMIP5 model ensemble. *The Cryosphere*, *9*(5), 1943–1953. https://doi.org/10.5194/tc-9-1943-2015

Shiogama, H., Abe, M., & Tatebe, H. (2019). *MIROC MIROC6 model output prepared for CMIP6 ScenarioMIP*. Earth System Grid Federation. https://doi.org/10.22033/ESGF/CMIP6.898

Spinoni, J., Barbosa, P., Bucchignani, E., Cassano, J., Cavazos, T., Christensen, J. H., et al. (2020). Future global meteorological drought hot spots: A study based on CORDEX data. *Journal of Climate*, *33*(9), 3635–3661. https://doi.org/10.1175/JCLI-D-19-0084.1

Swann, A. L. S. (2018). Plants and drought in a changing climate. *Current Climate Change Reports*, *4*(2), 192–201. https://doi.org/10.1007/s40641-018-0097-y

Swann, A. L. S., Hoffman, F. M., Koven, C. D., & Randerson, J. T. (2016). Plant responses to increasing CO_2 reduce estimates of climate impacts on drought severity. *Proceedings of the National Academy of Sciences*, *113*(36), 10019–10024. https://doi.org/10.1073/pnas.1604581113

Swart, N. C., Cole, J. N., Kharin, V. V., Lazare, M., Scinocca, J. F., Gillett, N. P., et al. (2019a). *CCCma CanESM5 model output prepared for CMIP6 CMIP historical*. Earth System Grid Federation. https://doi.org/10.22033/ESGF/CMIP6.3610

Swart, N. C., Cole, J. N. S., Kharin, V. V., Lazare, M., Scinocca, J. F., Gillett, N. P., et al. (2019b). *CCCma CanESM5 model output prepared for CMIP6 ScenarioMIP*. https://doi.org/10.22033/ESGF/CMIP6.1317

Tang, Y., Rumbold, S., Ellis, R., Kelley, D., Mulcahy, J., Sellar, A., et al. (2019). *MOHC UKESM1.0-LL model output prepared for CMIP6 CMIP*. Earth System Grid Federation. https://doi.org/10.22033/ESGF/CMIP6.1569

Tatebe, H., & Watanabe, M. (2018). *MIROC MIROC6 model output prepared for CMIP6 CMIP*. https://doi.org/10.22033/ESGF/CMIP6.881

Thomas, B. F., Famiglietti, J. S., Landerer, F. W., Wiese, D. N., Molotch, N. P., & Argus, D. F. (2017). GRACE groundwater drought index: Evaluation of California central valley groundwater drought. *Remote Sensing of Environment*, *198*, 384–392. https://doi.org/10.1016/j.rse.2017.06.026

Ting, M., Seager, R., Li, C., Liu, H., & Henderson, N. (2018). Mechanism of future spring drying in the Southwestern United States in CMIP5 Models. *Journal of Climate*, *31*(11), 4265–4279. https://doi.org/10.1175/JCLI-D-17-0574.1

Tronstad, R., & Feuz, D. M. (2002). Impacts of the 2002 drought on western ranches and public land policies. In Western Economics Forum. (Vol. 1, pp. 19–24).

Udall, B., & Overpeck, J. (2017). The twenty-first century Colorado River hot drought and implications for the future. *Water Resources Research*, *53*(3), 2404–2418. https://doi.org/10.1002/2016WR019638

Ukkola, A. M., De Kauwe, M. G., Roderick, M. L., Abramowitz, G., & Pitman, A. J. (2020). Robust future changes in meteorological drought in CMIP6 projections despite uncertainty in precipitation. *Geophysical Research Letters*, *47*(11), e2020GL087820. https://doi.org/10.1029/2020GL087820

Voldoire, A. (2018). *CNRM-CERFACS CNRM-CM6-1 model output prepared for CMIP6 CMIP*. https://doi.org/10.22033/ESGF/CMIP6.1375

Voldoire, A. (2019). *CNRM-CERFACS CNRM-CM6-1 model output prepared for CMIP6 ScenarioMIP*. Earth System Grid Federation. https://doi.org/10.22033/ESGF/CMIP6.1384

Wieners, K.-H., Giorgetta, M., Jungclaus, J., Reick, C., Esch, M., Bittner, M., et al. (2019a). *MPI-M MPIESM1.2-LR model output prepared for CMIP6 CMIP*. Earth System Grid Federation. https://doi.org/10.22033/ESGF/CMIP6.742

Wieners, K.-H., Giorgetta, M., Jungclaus, J., Reick, C., Esch, M., Bittner, M., et al. (2019b). *MPI-M MPIESM1.2-LR model output prepared for CMIP6 ScenarioMIP*. Earth System Grid Federation. https://doi.org/10.22033/ESGF/CMIP6.793

Williams, A. P., Allen, C. D., Macalady, A. K., Griffin, D., Woodhouse, C. A., Meko, D. M., et al. (2013). Temperature as a potent driver of regional forest drought stress and tree mortality. *Nature Climate Change*, *3*(3), 292–297. https://doi.org/10.1038/nclimate1693

Williams, A. P., Cook, E. R., Smerdon, J. E., Cook, B. I., Abatzoglou, J. T., Bolles, K., et al. (2020). Large contribution from anthropogenic warming to an emerging North American megadrought. *Science*, *368*(6488), 314–318. https://doi.org/10.1126/science.aaz9600

Williams, A. P., Seager, R., Abatzoglou, J. T., Cook, B. I., Smerdon, J. E., & Cook, E. R. (2015). Contribution of anthropogenic warming to the 2012–2014 California drought. *Geophysical Research Letters*, *42*(16), 6819–6828. https://doi.org/10.1002/2015GL064924

Woodhouse, C. A., Pederson, G. T., Morino, K., McAfee, S. A., & McCabe, G. J. (2016). Increasing influence of air temperature on upper Colorado River streamflow. *Geophysical Research Letters*, *43*(5), 2174–2181. https://doi.org/10.1002/2015GL067613

Wu, T., Chu, M., Dong, M., Fang, Y., Jie, W., Li, J., & Zhang, Y. (2018). *BCC BCC-CSM2MR model output prepared for CMIP6 CMIP historical*. https://doi.org/10.22033/ESGF/CMIP6.2948

Xiao, M., Koppa, A., Mekonnen, Z., Pagán, B. R., Zhan, S., Cao, Q., et al. (2017). How much groundwater did california's central valley lose during the 2012–2016 drought? *Geophysical Research Letters*, *44*(10), 4872–4879. https://doi.org/10.1002/2017GL073333

Xiao, M., Udall, B., & Lettenmaier, D. P. (2018). On the causes of declining colorado river streamflows. *Water Resources Research*, *54*(9), 6739–6756. https://doi.org/10.1029/2018WR023153

Xin, X., Wu, T., Shi, X., Zhang, F., Li, J., Chu, M., et al. (2019). *BCC BCC-CSM2MR model output prepared for CMIP6*. System Grid Federation. https://doi.org/10.22033/ESGF/CMIP6.1732

Yukimoto, S., Koshiro, T., Kawai, H., Oshima, N., Yoshida, K., Urakawa, S., et al. (2019a). *MRI MRI-ESM2.0 model output prepared for CMIP6 CMIP*. https://doi.org/10.22033/ESGF/CMIP6.621

Yukimoto, S., Koshiro, T., Kawai, H., Oshima, N., Yoshida, K., Urakawa, S., et al. (2019b). *MRI MRI-ESM2.0 model output prepared for CMIP6 ScenarioMIP*. Earth System Grid Federation. https://doi.org/10.22033/ESGF/CMIP6.638

Zhao, C., Brissette, F., Chen, J., & Martel, J.-L. (2020). Frequency change of future extreme summer meteorological and hydrological droughts over North America. *Journal of Hydrology*, *584*, 124316. https://doi.org/10.1016/j.jhydrol.2019.124316

Ziehn, T., Chamberlain, M., Lenton, A., Law, R., Bodman, R., Dix, M., et al. (2019a). *CSIRO ACCESS-ESM1.5 model output prepared for CMIP6 CMIP*. Earth System Grid Federation. https://doi.org/10.22033/ESGF/CMIP6.2288

Ziehn, T., Chamberlain, M., Lenton, A., Law, R., Bodman, R., Dix, M., et al. (2019b). *CSIRO ACCESS-ESM1.5 model output prepared for CMIP6 ScenarioMIP*. Earth System Grid Federation. https://doi.org/10.22033/ESGF/CMIP6.2291